

A Raman-Gas Spectral Compressor for High-Energy Femtosecond Laser Pulses

ZEGUI WANG,¹ YUNLONG MO,² ZAITIAN DONG,² WANHONG YIN,² WEI CAO,^{1,*}

¹*School of Physics and Wuhan National Laboratory for Optoelectronics, Huazhong University of Science and Technology, Wuhan 430074, China*

²*Xi'an Institute of Applied Optics, Xi'an 710065, China*

[*weicao@hust.edu.cn](mailto:weicao@hust.edu.cn)

Abstract: We propose and experimentally demonstrate an efficient spectral compression technique for optical laser fields. By exploiting the Raman effect of molecular gas confined in a hollow-core capillary we achieve spectral compression of millijoule-level femtosecond laser pulses, attaining a compression ratio up to 14 times with near 50% efficiency. This method also features precise and continuous tunability of the central wavelength. Furthermore, we directly extend this scheme to an ambient air medium, realizing a simple high-energy femtosecond laser spectral tuning apparatus. The developed technique has promising applications in advanced manufacturing, bio-imaging, and material spectroscopic studies.

1. Introduction

Selective extraction of specific wavelength components from a broadband light source is essential for many advanced applications. High-resolution imaging^{[1][2][3][4]}, for example, demands light sources with high temporal coherence (i.e., narrow spectral bandwidth). Precision laser processing of certain materials also requires tailored wavelengths due to their strong absorption at specific spectral regions^{[5][6]}. Furthermore, spectroscopic techniques rely on continuous wavelength scanning to acquire material response spectra, placing stringent demands on spectral selectivity and tunability of the source. Conventional wavelength-selection methods, such as optical filters and programmable pulse shapers^{[7][8]} (e.g., DAZZLER), often suffer from substantial energy loss despite their effectiveness in spectral filtering. Alternatively, nonlinear frequency conversion processes—including harmonic generation^{[9][10][11]}, sum-frequency, and difference-frequency generation^{[12][13][14]}—can reshape spectra, but they generally require high-power pump lasers and exhibit limited conversion efficiency.

Nonlinear spectral compression(SC) has recently emerged as a promising approach to generating narrowband pulses^{[15][16][17]}. It refers to the technique of concentrating spectral energy near a specific wavelength by leveraging nonlinear effects, which entails minimal energy loss. By coupling pre-chirped pulses with nonlinear effects such as self-phase modulation (SPM), high compression ratios can be achieved with good efficiency^{[18][19]}. For instance, NOUR DAHER et al. demonstrated SC in a multi-pass cell using fused silica^[20]. However, due to the low nonlinear damage threshold of fused silica, this approach is difficult to scale to millijoule-level pulses. Extensive research has been conducted using various fibers, including single-mode fibers^{[16][21]}, photonic crystal fibers^{[22][23][24]}, and dispersion-increasing fiber^{[25][26]}. However, the small core size and low damage threshold of single-mode fibers, photonic crystal fibers restrict this method to microjoule-level pulse energies and lacks the ability to tune the wavelength, thereby limiting its practical scope.

To overcome these limitations, we propose and demonstrate a SC technique suitable for millijoule-level femtosecond lasers. Our approach employs a hollow-core capillary filled with molecular gas as the nonlinear medium. Injecting high-energy femtosecond pulses into the capillary stimulates nonlinear processes including SPM^{[27][28]} and stimulated Raman scattering(SRS)^{[28][29][30][31]}. By matching the pulse pre-chirp to the nonlinear phase

accumulation, efficient and wavelength-tunable SC is realized. Numerical simulations based on the nonlinear Schrödinger equation^{[29][34][35]} confirm that the Raman response introduces a time-domain quadratic phase, which can be compensated via pre-chirping to achieve effective spectral focusing.

Experimentally, using N₂O at 0.1 bar, we compressed pulses from 1.38 mJ with 60 nm bandwidth to 1.02 mJ with 5.81 nm bandwidth, where the compressed spectral peak(CSP) contained 51.11% of the energy. We further extended the scheme to ambient air^{[32][33]} as the nonlinear medium, obtaining narrowband outputs of 0.35 mJ with 6.68 nm bandwidth. This air-based implementation significantly simplifies the setup while maintaining performance, and holds promising potential for future applications.

2. Experimental results Results and Discussion

A schematic of the experimental setup is shown in Fig. 1(a). Spectral compression was achieved using a hollow-core capillary with an inner diameter of 400 μm . The large core size enabled efficient coupling of millijoule-level laser pulses. The pulses were generated by a mode-locked Ti:sapphire amplifier system with the following output parameters: central wavelength of 785 nm, spectral width of 60 nm, and repetition rate of 1 kHz. The chirped-pulse amplification system included a Treacy-type grating-pair compressor, which allowed precise control of the pulse chirp via fine adjustment of the grating separation.

A pre-chirped femtosecond laser pulse was focused into the hollow-core capillary filled with molecular gas. By adjusting the incident pulse energy, gas pressure, and initial pre-chirp, the output pulse exhibited clear spectral compression, with most of the pulse energy concentrated into a narrow spectral peak whose position could be precisely tuned across the original bandwidth, as shown in Figs. 1(b) and (c). Detailed tuning characteristics will be discussed in a later section.

Applying a strong negative chirp temporally broadened the pulses to several hundred femtoseconds. On this timescale, self-phase modulation and ionization effects were significantly suppressed, allowing the pulses to maintain high-quality fundamental-mode propagation. Under these conditions, the overall transmission efficiency of the capillary system was approximately 75%, a value that already includes insertion losses from both the anti-reflection-coated input window and the uncoated output window. The beam profile confirmed a high-purity fundamental transverse mode. As shown in Fig. 1(d), the intensity profile of the capillary output, recorded with an industrial camera, displays a uniform, near-Gaussian distribution.

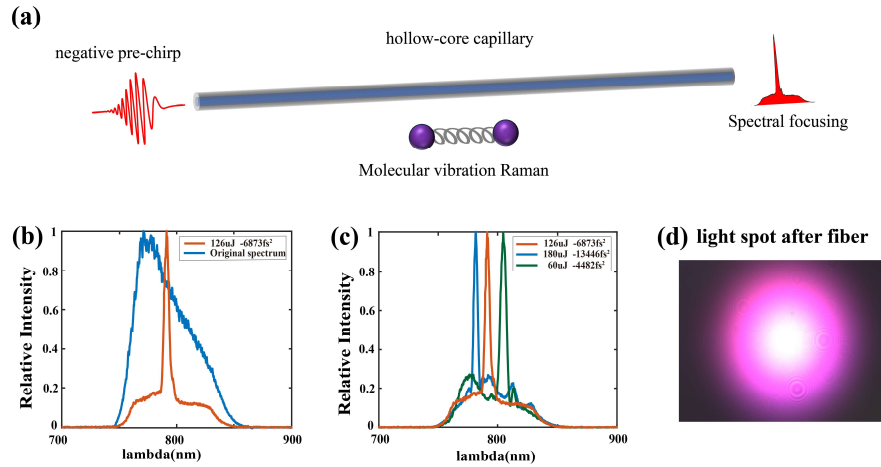


Fig. 1. (a) Schematic of SC based on molecular vibrational SRS effect in a hollow-core capillary. (b) Comparison of the input and output spectrum of hollow-core capillary. (c) Compressed spectrum under different incident pulse energies and pre-chirp values, illustrating the tunability of the CSP wavelength. (d) Spatial intensity distribution of the output laser beam from the hollow-core capillary, recorded with an industrial camera.

Figure 2 presents the experimental results of spectral compression as a function of chirp for different gas species at a pressure of 1 bar. For molecular gases such as N₂ and N₂O (Fig. 2(a) and (c)), when the input pulse is near the Fourier-transform limit (small chirp values), self-phase modulation dominates during propagation in the capillary, resulting in a broad supercontinuum spectrum. As negative chirp is introduced, the output pulse energy becomes concentrated into a narrow spectral peak. With increasing absolute chirp, the compressed spectral peak (CSP) shifts progressively toward higher frequencies. Although the overall trend is similar for both N₂ and N₂O, the amount of pre-chirp required for effective spectral compression is notably larger for N₂O. For example, the optimum CSP full-width at half-maximum (FWHM) is 6.68 nm at a chirp of -3884 fs² for N₂, compared to 4.81 nm at -6873 fs² for N₂O. Moreover, N₂O exhibits a smoother spectral baseline compared to the oscillating baseline observed for N₂.

For comparison, similar experiments were performed with atomic gases. As shown in Fig. 2(e), the spectral response of Ar does not yield a clean CSP over the entire chirp tuning range. The spectrum corresponding to the maximum achievable compression ratio is plotted in Fig. 2(f); it displays prominent sidebands and residual broadening, both of which reduce energy concentration. Compressed spectra in atomic gases consistently showed pronounced sidebands under all tested conditions of pressure, energy, and chirp. Consequently, achieving high-quality spectral compression in atomic gases remains challenging.

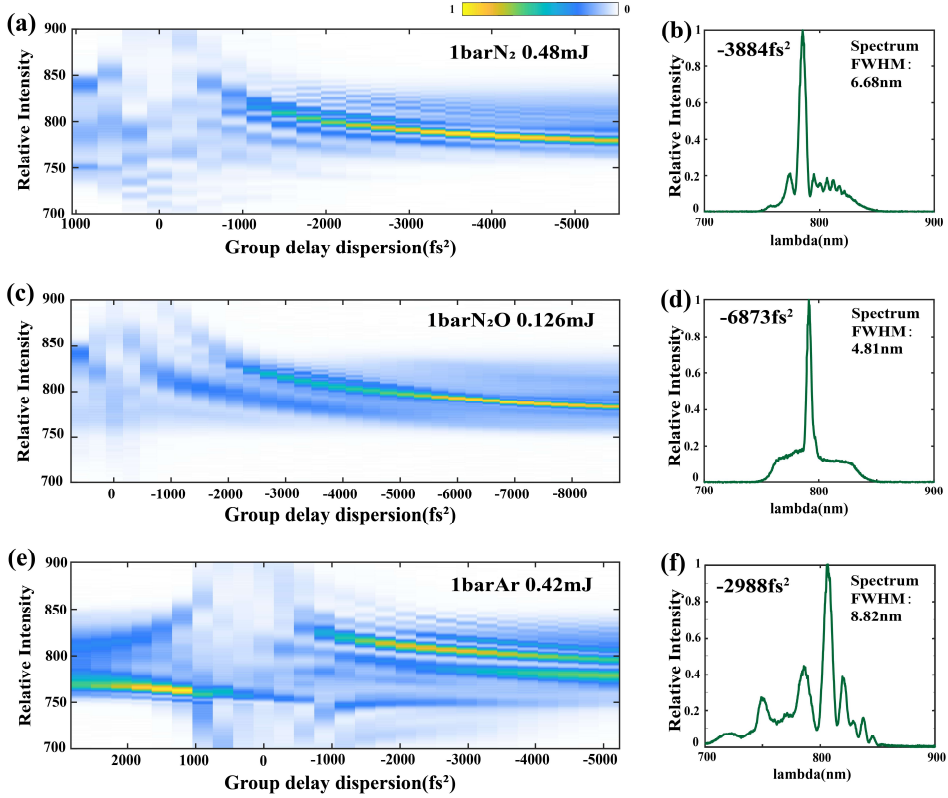


Fig. 2. (a) Experimental results of SC for different gas species. Spectrogram with chirp for (a) N_2 , (c) N_2O , and (e) Ar, respectively. The color bar above indicates relative intensity, with the corresponding gas pressure and incident pulse energy labeled in the upper-right corner. Spectrum corresponding to the maximum achievable compression ratio from the left column, for (b) N_2 , (d) N_2O , and (f) Ar, respectively.

The comparative study shown in Figure 2 indicates that N_2O exhibits better spectral compression performance in terms of compression ratio, spectral purity, and conversion efficiency. To further investigate its behavior, we examined the spectral evolution versus chirp under different incident pulse energies for N_2O gas; the results are presented in Fig. 3. The left-hand panels (a, c, e) correspond to incident pulse energies of 60 μJ , 126 μJ , and 180 μJ , respectively. As the energy increases, the amount of chirp required to achieve effective spectral compression also rises accordingly. For each energy level, the spectrum corresponding to the narrowest FWHM of the CSP is shown in the right-hand panels (b, d, f). Compared with the low- and high-energy cases, the spectrum obtained at 126 μJ displays a cleaner and smoother baseline. The FWHM of the CSP gradually narrows with increasing energy, reaching 4.28 nm at 180 μJ . Compared with the initial bandwidth of 60 nm, this corresponds to a compression ratio of about 14. Moreover, the central wavelength of the CSP blueshifts with increasing energy, shifting from 798 nm (60 μJ) to 791.3 nm (126 μJ) and finally to 781.3 nm (180 μJ). These experiments demonstrate that by adjusting both the incident pulse energy and the chirp, active control can be achieved over both the central wavelength (as illustrated in Fig. 1c) and the spectral width of the CSP.

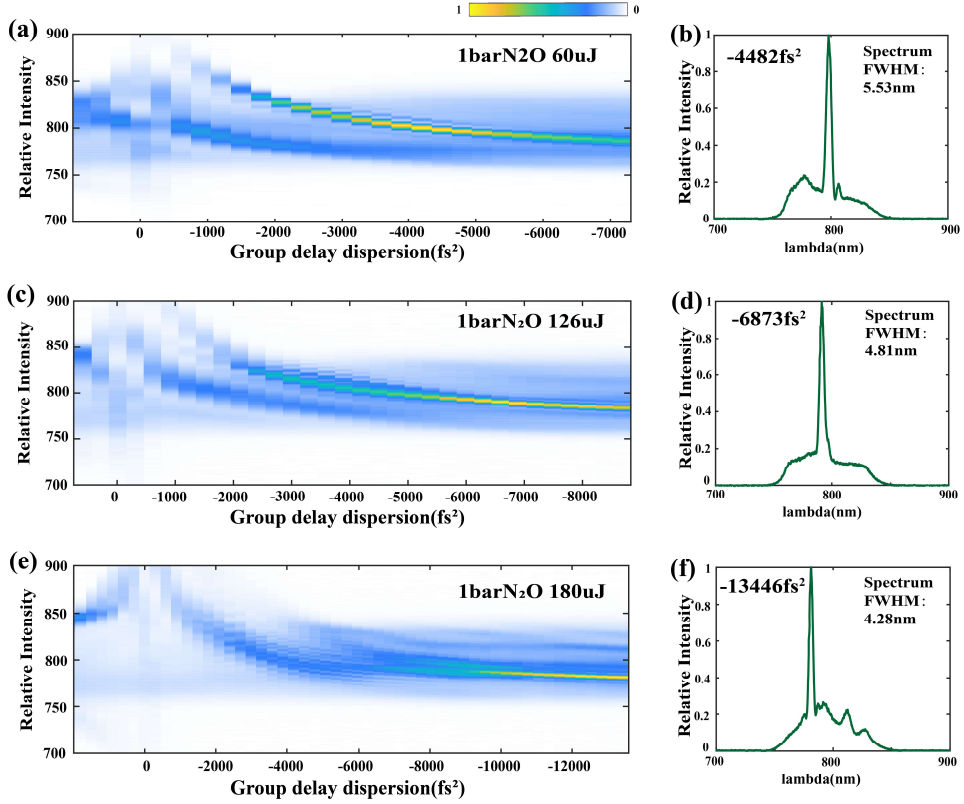


Fig. 3. Same as Fig 2. But for 1bar N₂O with incident pulse energy of (a)60uJ (c)126uJ (e)180uJ.

To further investigate the energy-scaling capability of the present method, experiments were conducted at different gas pressures. Figure 4 shows the compressed spectra of N₂O at 1 bar, 0.5 bar, 0.3 bar, and 0.1 bar, with the corresponding chirp values indicated in the figure. The results show that as the pressure decreases, the optimal pre-chirp required for compression is reduced, while the FWHM of the CSP gradually increases and its energy fraction improves. Moreover, the incident pulse energy needed for effective compression rises significantly, yet the spectral profile remains similar in shape. At the lowest pressure tested (0.1 bar), an incident pulse energy of up to 1.38 mJ could be applied, yielding a conversion efficiency of 51.11% into the CSP. These findings demonstrate that reducing the gas pressure allows the system to accommodate higher-energy laser pulses effectively. The maximum pulse energy achievable in the current setup is primarily limited by the inner diameter and damage threshold of the capillary used. Scaling to even higher energies would require capillaries with larger core sizes and improved damage resistance.

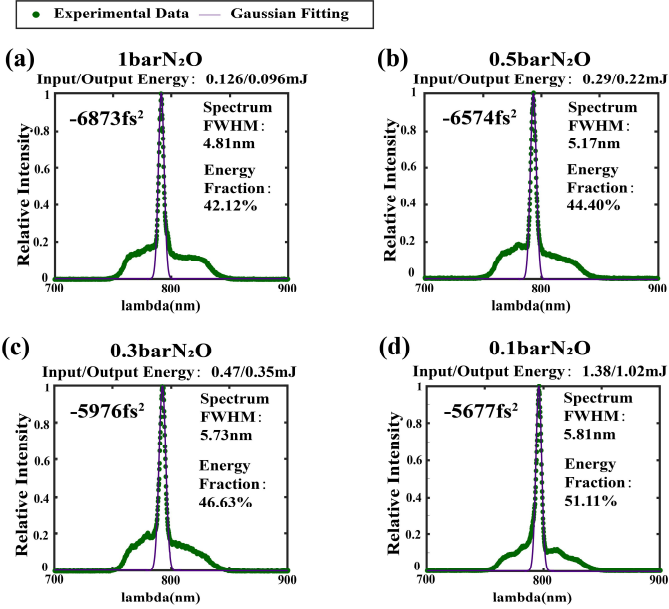


Fig. 4. Experimental results of SC in N₂O under different gas pressures: (a) 1 bar, (b) 0.5 bar, (c) 0.3 bar, (d) 0.1 bar. In each panel, the green curve represents the measured spectrum obtained at the optimal pulse energy for the corresponding pressure, while the purple curve denotes the corresponding Gaussian fit. The pre-chirp applied is indicated in the upper-left corner of each plot. Spectral FWHM and energy fraction are listed on the right side of each spectrum.

3. Numerical simulation and mechanism analysis

To clarify the physical mechanism underlying our experiment, we performed a series of numerical simulations by solving the nonlinear Schrödinger equation using the split-step Fourier method^{[29][34][35]}. The simulation model accounted for Kerr nonlinearity (including SPM and self-steepening) in atomic gases, while for molecular gases, stimulated Raman scattering (SRS) was additionally incorporated via a harmonic oscillator model^{[29][36][37]}. Parameters such as Kerr coefficients, Raman-active vibrational frequencies, and Raman relaxation times for Ar, N₂, and N₂O were taken from reported values under long-pulse conditions [ref.30]. Because of the strong pre-chirp applied and the resulting pulse durations of several hundred femtoseconds, the peak power remained relatively low; therefore, ionization and multiphoton absorption were neglected in the simulations.

Simulations corresponding to the experimental conditions of Fig. 2 were first carried out, as shown in Fig. 5. The simulation parameters were set as follows: capillary length 1 m, focal spot diameter 200 μ m, gas pressure 1 bar, and pulse energies of 0.5 mJ for Ar and N₂ and 0.15 mJ for N₂O, closely matching the experimental settings. The top row of Fig. 5 presents the simulated results for Ar, indicating that effective spectral compression is difficult to achieve when only the Kerr effect is present. The middle row shows the results for N₂. Consistent with the experimental observations, pronounced spectral compression occurs under large chirp, and the central wavelength of the compressed spectral peak (CSP) blueshifts with increasing chirp. However, the spectral background noise in the simulation is considerably lower than in the experiment, suggesting room for further optimization in the experimental setup. The bottom row displays the results for N₂O. Under matched conditions with larger chirp, the simulation yields a narrower Raman-compressed peak, a trend clearly validated by the experiment. Based on these findings, spectral compression in atomic gases relying solely on the Kerr effect appears

largely ineffective, whereas the Raman effect is likely a key mechanism for achieving high-quality spectral compression.

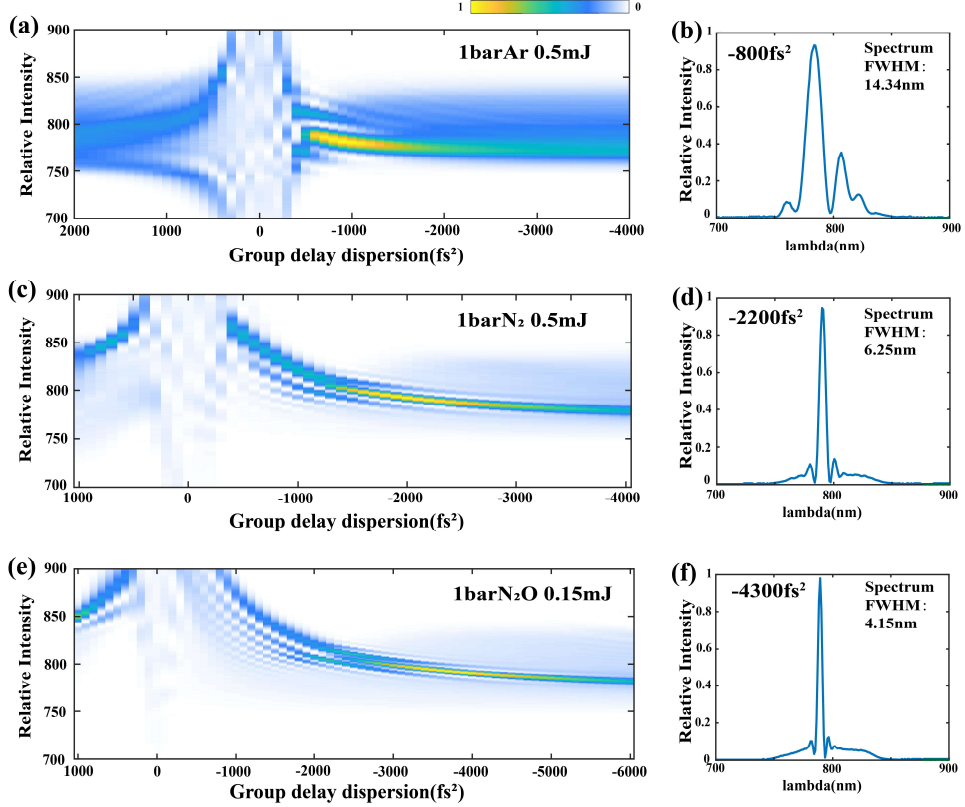


Fig. 5. Same as Fig. 2 but for numerical simulation.

The temporal phase dynamics before and after the laser-molecule interaction are analyzed and the results are shown in Fig. 6. Specifically, a simulation was conducted for a Fourier-transform-limited 30-fs Gaussian pulse with 0.1 mJ energy and a pre-chirp of -5000 fs^2 , propagating over 1 m in N₂O at a pressure of 1 bar. The temporal intensity and phase of the pulse before and after capillary are presented in Fig. 6(a) and (c), respectively. To intuitively illustrate the physical mechanism of SC, we used the instantaneous wavelength corresponding to the temporal phase for representation. In this depiction, the pulse clearly exhibits a negatively chirped structure with "shorter wavelengths leading and longer wavelengths trailing." as shown in Fig. 6(a). Upon propagation through the capillary, the temporal phase modulation provided by the molecular gas in our scheme causes the instantaneous wavelengths at both the leading and trailing edges of the pulse to shift toward the central wavelength. This leads to a high concentration of energy around specific wavelengths, ultimately achieving SC in the frequency domain, as shown in the results of Fig. 6(d). We show the modulating effects of the Kerr and Raman effects on the temporal phase, calculated at a step size of 1 mm, are presented in Fig. 6(b). For pulses with large chirp and durations of several hundred femtoseconds, the SRS effect plays a dominant role over the Kerr effect in modulating the temporal phase, as evidenced by the results in Fig. 6(b).

In conventional temporal compression methods for Ultrafast laser pulses, it is typically necessary to first broaden the spectrum to support a narrower Fourier-transform-limited

temporal structure. It is then necessary to compensate for the temporal quadratic phase introduced by spectral broadening, thereby compressing the pulse duration as close as possible to the Fourier limit. The SC technique we propose follows a similar principle: first, the pulse is temporally broadened via pre-chirping. Then, analogous to how a spatial lens focuses a beam with a quadratic phase, the nonlinear effect of the gas within the capillary acts like a "temporal lens," applying a compensatory quadratic phase modulation to the pulse, ultimately achieving spectral focusing.

SPM is closely linked to the instantaneous intensity, for pulses with significant pre-chirp, this results in a phase compensation time window that is confined solely to the high-energy region near the peak of the pulse. To compensate for the quadratic phase at the pulse edges would require even higher intensities, at which point plasma effects, multiphoton absorption, and other phenomena become unavoidable. These introduce temporal phase distortion, thereby degrading the compression efficiency. In contrast, the SRS effect in molecular gases exhibits a relatively long relaxation time than SPM in atomic gases, providing a broader temporal compensation window. Furthermore, molecular gases generally exhibit a larger third-order Raman nonlinear coefficient, requiring lower instantaneous intensity for effective phase modulation. This helps avoid disturbed by ionization and Kerr effects on the temporal phase. Compared to N₂, N₂O possesses a longer Raman relaxation time and a larger Raman nonlinear coefficient, enabling significantly improved performance in SC.

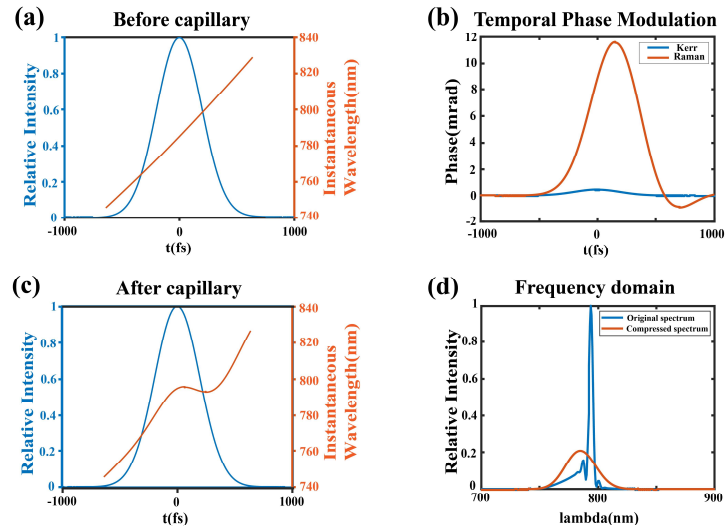


Fig. 6. Numerical simulation results of SC. (a) Temporal characteristics of a Fourier-transform-limited 30-fs Gaussian pulse with a chirp of -5000 fs^2 applied. The blue curve represents the temporal intensity, and the orange curve indicates the instantaneous wavelength. (b) Temporal phase modulation induced by nonlinear effects over a 1-mm propagation step. The orange line corresponds to the SRS effect, and the blue line corresponds to the Kerr effect. (c) Temporal structure and phase of the pulse after propagation through a 1-m N₂O-filled capillary. (d) Spectral evolution: the orange curve shows the original spectrum, and the blue curve shows the compressed spectrum.

4. Experiment in air medium

Considering that ambient air consists of approximately 78% nitrogen and 21% oxygen—both of which are Raman-active molecular gases—a significantly simplified spectral compression setup can be realized by using air as the nonlinear medium. By retaining only the capillary mount and alignment stages, experiments were directly performed in air. Eliminating the energy losses associated with input and output sealed windows improved the overall

transmission efficiency of the setup from approximately 75% to around 80%. The experimental results for SC obtained in air are shown in Fig. 7. These results are highly similar to those obtained in a pure N₂ environment, as presented in Figure 2. This simplified setup design demonstrates that the SC method remains effective without the need for complex gas regulation, which is beneficial for promoting its adoption in a wider range of practical applications.

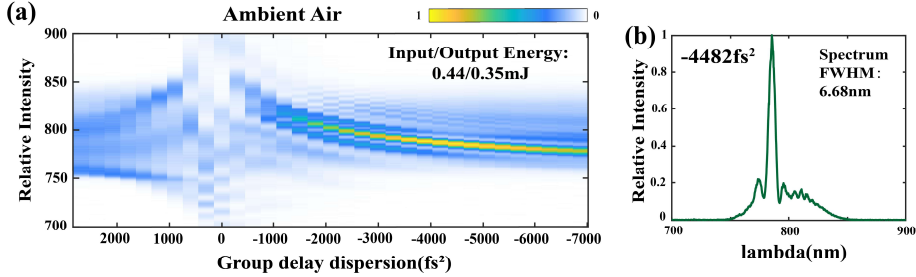


Fig. 7. Same as Fig. 2 but for experiment in ambient air medium.

5. Summary and Prospect

A spectral compression method for millijoule-level femtosecond laser pulses is demonstrated using a hollow-core capillary. The approach utilizes stimulated Raman scattering in molecular gases to impart temporal phase modulation to negatively pre-chirped pulses, ultimately achieving spectral focusing in the frequency domain. Through systematic experiments and numerical simulations, we compared the performance of atomic gases (Ar) with molecular gases (N₂, N₂O), and thoroughly investigated the synergistic effects of gas pressure, pulse energy, and chirp on the compression characteristics.

Key results include spectral compression in N₂O at 0.1 bar with a pulse energy of 1.02 mJ, delivering a compressed spectral peak (CSP) containing 51.11 % of the pulse energy and a spectral width of 5.81 nm. Under 1 bar N₂O at 0.18 mJ, a compression ratio of 14 was achieved, yielding a CSP width of 4.28 nm while allowing continuous tuning of the CSP center wavelength across the original spectrum. Furthermore, by simplifying the setup to operate in ambient air—eliminating sealed windows and gas cells—spectral compression to 6.68 nm was obtained with 0.35 mJ pulse energy, significantly reducing system complexity and improving practicality. This work demonstrates a robust, tunable, and efficient approach to spectral compression of high-energy femtosecond pulses, with promising potential for applications in spectral tailoring and imaging.

Funding. This work is financially supported by the National Key Development Program for Basic Research of China (Grant Nos. 2024YFE0205800), the National Natural Science Foundation of China (Grant Nos. 12274158)

Disclosures. The authors declare no competing interests.

Data availability. Data underlying the results presented in this paper are not publicly available at this time but may be obtained from the authors upon reasonable request.

References

1. Bhargava A, Sachdeva A, Sharma K, et al. Hyperspectral imaging and its applications: A review[J]. *Heliyon*, 2024, 10(12).
2. Lynch P G, Das A, Alam S, et al. Mastering femtosecond stimulated Raman spectroscopy: A practical guide[J]. *Acs Physical Chemistry Au*, 2023, 4(1): 1-18.
3. Drexler W, Liu M, Kumar A, et al. Optical coherence tomography today: speed, contrast, and multimodality[J]. *Journal of biomedical optics*, 2014, 19(7): 071412-071412.

4. Wang Z, You Q, Gao Y, et al. High-precision spatiotemporal profiler of femtosecond laser pulses[J]. *Photonics Research*, 2025, 13(6): 1666-1673.
5. Malinauskas M, Žukauskas A, Hasegawa S, et al. Ultrafast laser processing of materials: from science to industry[J]. *Light: Science & Applications*, 2016, 5(8): e16133-e16133.
6. Linz N, Freidank S, Liang X X, et al. Wavelength dependence of femtosecond laser-induced breakdown in water and implications for laser surgery[J]. *Physical Review B*, 2016, 94(2): 024113.
7. Weiner A M. Ultrafast optical pulse shaping: A tutorial review[J]. *Optics Communications*, 2011, 284(15): 3669-3692.
8. Verluise F, Laude V, Cheng Z, et al. Amplitude and phase control of ultrashort pulses by use of an acousto-optic programmable dispersive filter: pulse compression and shaping[J]. *Optics letters*, 2000, 25(8): 575-577.
9. Konforty N, Cohen M I, Segal O, et al. Second harmonic generation and nonlinear frequency conversion in photonic time-crystals[J]. *Light: Science & Applications*, 2025, 14(1): 152.
10. Zeng Q, Yang X, Deng Y, et al. All-optical spatiotemporal oscilloscope for few-cycle optical waveform[J]. *Advanced Photonics*, 2025, 7(1): 016001-016001.
11. Mo Y, Cao W, Xu H, et al. Few-cycle optical pulse characterization under phase-mismatching[J]. *Optics Letters*, 2021, 46(3): 548-551.
12. Dogadov O, Trovatello C, Yao B, et al. Parametric nonlinear optics with layered materials and related heterostructures[J]. *Laser & Photonics Reviews*, 2022, 16(9): 2100726.
13. Xu L, Takahashi E J. Dual-chirped optical parametric amplification of high-energy single-cycle laser pulses[J]. *Nature Photonics*, 2024, 18(1): 99-106.
14. Mi K, Cao W, Xu H, et al. Perturbed ac stark effect for attosecond optical-waveform sampling[J]. *Physical Review Applied*, 2020, 13(1): 014032.
15. Sukiasyan M, Avetisyan V, Kutuzyan A. Spectral self-compression of chirp-free pulses in anomalously dispersive optical fibers[C]//*Photonics*. MDPI, 2023, 10(11): 1207.
16. Oberthaler M, Höpfel R A. Special narrowing of ultrashort laser pulses by self-phase modulation in optical fibers[J]. *Applied Physics Letters*, 1993, 63(8): 1017-1019.
17. Toneyan H, Zeytunyan A, Zadoyan R, et al. Classic, all-fiber, and similaritonic techniques of spectral compression[C]//*Journal of Physics: Conference Series*. IOP Publishing, 2016, 672(1): 012016.
18. Finot C, Boscolo S. Design rules for nonlinear spectral compression in optical fibers[J]. *Journal of the Optical Society of America B*, 2016, 33(4): 760-767.
19. Wu J, Li Q. Highly efficient self-similar spectral compression of hyperbolic secant pulses enhanced by pre-chirping in nonlinear fibres[J]. *Journal of Optics*, 2019, 21(8): 085503.
20. Daher N, Guichard F, Délen X, et al. Spectral compression in a multipass cell[J]. *Optics Express*, 2020, 28(15): 21571-21577.
21. Washburn B R, Buck J A, Ralph S E. Transform-limited spectral compression due to self-phase modulation in fibers[J]. *Optics Letters*, 2000, 25(7): 445-447.
22. Limpert J, Deguil-Robin N, Manek-Hönniger I, et al. High-power picosecond fiber amplifier based on nonlinear spectral compression[J]. *Optics Letters*, 2005, 30(7): 714-716.
23. Andresen E R, Thøgersen J, Keiding S R. Spectral compression of femtosecond pulses in photonic crystal fibers[J]. *Optics letters*, 2005, 30(15): 2025-2027.
24. Sidorov-Biryukov D A, Fernandez A, Zhu L, et al. Spectral narrowing of chirp-free light pulses in anomalously dispersive, highly nonlinear photonic-crystal fibers[J]. *Optics Express*, 2008, 16(4): 2502-2507.
25. Lin Y S, Huang C B. Large-scale and structure-tunable laser spectral compression in an optical dispersion-increasing fiber[J]. *Optics Express*, 2017, 25(15): 18024-18030.
26. Szewczyk O, Łaszczyk Z, Soboń G. Spectral compression and amplification of ultrashort pulses tunable in the 1650-1900 nm wavelength range[J]. *Optics & Laser Technology*, 2023, 164: 109465.
27. Stolen R H, Lin C. Self-phase-modulation in silica optical fibers[J]. *Physical Review A*, 1978, 17(4): 1448.
28. Weiner A M, Heritage J P, Stolen R H. Self-phase modulation and optical pulse compression influenced by stimulated Raman scattering in fibers[J]. *Journal of the Optical Society of America B*, 1988, 5(2): 364-372.
29. Mo Y, Cao W, Wang Z, et al. Spectral tuning of a broadband optical pulse via stimulated Raman scattering of a prealigned molecule[J]. *Physical Review A*, 2022, 105(4): 043504.
30. Beeter J E, Nrisimhamurti M, Truong T C, et al. Multi octave supercontinuum generation and frequency conversion based on rotational nonlinearity[J]. *Science Advances*, 2020, 6(34): eabb5375.
31. Carpeggiani P A, Coccia G, Fan G, et al. Extreme Raman red shift: ultrafast multimode nonlinear space-time dynamics, pulse compression, and broadly tunable frequency conversion[J]. *Optica*, 2020, 7(10): 1349-1354.
32. Dogariu A, Michael J B, Scully M O, et al. High-gain backward lasing in air[J]. *Science*, 2011, 331(6016): 442-445.
33. Xu H, Lötstedt E, Iwasaki A, et al. Sub-10-fs population inversion in N2+ in air lasing through multiple state coupling[J]. *Nature communications*, 2015, 6(1): 8347.
34. Weideman J A C, Herbst B M. Split-step methods for the solution of the nonlinear Schrödinger equation[J]. *SIAM Journal on Numerical Analysis*, 1986, 23(3): 485-507.
35. Taha T R, Ablowitz M I. Analytical and numerical aspects of certain nonlinear evolution equations. II. Numerical, nonlinear Schrödinger equation[J]. *Journal of computational physics*, 1984, 55(2): 203-230.
36. Wang C S. Theory of stimulated Raman scattering[J]. *Physical Review*, 1969, 182(2): 482.

37. Headley III C, Agrawal G P. Unified description of ultrafast stimulated Raman scattering in optical fibers[J]. Journal of the Optical Society of America B, 1996, 13(10): 2170-2177.